

Conformal Carbon Coating on Hard Carbon Anode Derived from Propionaldehyde for Excellent Performance of Lithium-Ion Batteries

Longfeng Hu, Gang Cheng, Jingrun Ren, Fuming Wang*, Jianguo Ren*

BTR new energy materials inc., Shenzhen, China 518106

*E-mail: wfm@btrchina.com, renjianguo@btrchina.com

Received: 2 November 2018 / Accepted: 19 December 2018 / Published: 7 February 2019

Hard carbon anode material is one of the most promising candidates for next-generation lithium-ion batteries with high power performance. Nevertheless, the poor conductivity and low initial Coulombic efficiency largely impede its commercial implementation. Herein, we demonstrate the utilization of propionaldehyde as a new coating precursor for synthesizing a core-shell structured hard carbon material by a chemical vapor deposition (CVD) coating route. The surface of the hard carbon can be evenly coated with a thin carbon layer of 0.5~2 μm in thickness. The powder conductivity measurement shows that the coated carbon shell can effectively improve the conductivity of the hard carbon from 27.3 to 36.3 S cm^{-1} . Further, the resultant core-shell structured product shows enhanced lithium storage performance. Especially, the electrode with high areal mass loading of over 5 mg cm^{-2} can deliver a large reversible capacity of 404.3 mAh g^{-1} and a high initial Coulombic efficiency of 85.2 %, representative of the increment of 79.1 mAh g^{-1} and 10.1% with respect to the uncoated counterpart, respectively. Importantly, coupled with a commercial NCM523 cathode, the full battery (18650 type) displays excellent cyclic stability with a low capacity decay of $\sim 0.012\%$ per cycle over 800 charge-discharge cycles at high rates of 6C/6C. We suggest that the CVD coating treatment by using propionaldehyde as a carbon precursor is an effective method in improving the overall electrochemical properties of hard carbon anodes for lithium-ion batteries.

Keywords: hard carbon, core-shell structure, propionaldehyde, chemical vapor deposition, lithium-ion batteries.

1. INTRODUCTION

Lithium-ion batteries (LIBs) have been extensively utilized in various portable electronics in virtues of their high energy density and long cycle life. Recently, as the interest in electric vehicles and hybrid electric vehicles increases, the application of LIBs in the automobiles requires high power

performance [1, 2]. Graphitic carbons are the most widely and successfully used anode materials since they feature with excellent cyclic performance and high Coulombic efficiency. However, the commercial graphitic carbons have critical shortcomings in that their reversible capacities and power performances are limited [3]. Hence, it is urgent to develop novel and advanced anode materials for LIBs with a higher power density [4].

Hard carbon is one of the most promising alternatives owing to low cost, environmental friendliness, and non-toxicity. Meanwhile, hard carbon-based anodes also show high specific capacity, long-time cycling, and excellent low-temperature performance [5, 6]. Thus, the hard carbon materials have caught much attention in recent years, which are envisaged to replace graphite-based materials as the next-generation anode materials for the application of LIBs in the transportation sector. Various precursors are available in preparing the anodic hard carbons, including resin [7], polymers [8], fossil fuels [9], and biomasses [10, 11]. Due to the abundant lithium storage sites (such as edges, vacancies, and heteroatoms defects) of hard carbon, its reversible capacity can reach up above the theoretical capacity of graphite carbon materials. Nevertheless, the hard carbons usually exhibit poor initial Coulombic efficiency (ICE), which may be caused by the formation of the massive lithium clusters during lithiation [12]. In addition, the hydrogen atoms located on the surface of the hard carbon structures give rise to the change of electron cloud density in the peripheral carbon atoms, resulting in severe voltage hysteresis [13]. Furthermore, the inhomogeneous potential/current distribution on the hard carbon electrodes reduce the lithium capacity since the hard carbon materials usually exhibit relatively poor electronic conductivity [14].

One effective method to circumvent the aforementioned issues might be to fabricate a core-shell structure. The outside shells not only create the highly conductive connections between individual active particles, but also provide a protective layer to impede the direct exposure and contact of the materials with the defect-rich surface to the electrolyte, consequently leading to enhanced capacity and ICE. Some strategies have been proposed to prepare the core-shell structured hard carbons. For example, Lee's group has applied a solid-phase cladding route to deposit a soft carbon layer onto the surface of a hard carbon material by employing polyvinylchloride [15] or coal-tar pitch [16] as the soft carbon precursor. This method had an advantage in the scale-up production of the materials, but it was hard to guarantee the homogeneous and complete coating due to weak interactions between the hard carbon cores and these soft carbon precursors in the solid phase system. Another widely used coating approach is chemical vapor deposition (CVD), of which the superficial deposition layers onto the hard carbon core are derived from the decomposition of gaseous small-molecule organics at high temperature. Although the CVD modification is beneficial for the formation of the outer coating layers with fewer defects, the method is dangerous since those gaseous small-molecule coating precursors such as CH_4 [17] and C_2H_4 [18] are inflammable and explosive. Therefore, developing an effective and user-friendly method for preparing the core-shell structured hard carbon materials with the uniform coating layers is still a great challenge.

With these perceptions, we herein prepared a core-shell structured hard carbon-based composite material by using pistachio shells as a carbon source and an oxygen-containing organics (propionaldehyde) as a novel CVD precursor. The influence of the carbon coating on the electrochemical properties of the materials was in detail investigated. It is found that the surface

coating can significantly improve the lithium storage performance of the biomass-derived hard carbon material.

2. EXPERIMENTAL

2.1 Material and methods

In this work, a biomass waster, pistachio nut shell, was used as the precursor of hard carbon. The purchased pistachio nut shells (Hubei Province, China) were pre-carbonized at 500 °C in tube furnace under N₂ (purity 99.99%) atmosphere. Then, the resultant carbonaceous materials were smashed into the powders with the median diameter (D50) of 9 μm. The powders were soaked in diluted HCl and DI water to remove the impurities. Afterwards, the CVD coating modification was carried out at 800 °C under N₂ atmosphere, using propionaldehyde as the coating precursor. Finally, the black product was collected after further calcination at 1000 °C for 2 h with a ramping rate of 3 °C min⁻¹, and it was denoted as PSC-C. For comparison, an uncoated hard carbon (denoted as PSC) as the control sample was also prepared using the same procedure but without CVD treatment.

2.2 Materials characterization methods

The morphology and element distribution of the hard carbon materials were characterized on a scanning electron microscope (SEM, Hitachi Hitachi, S4800) combined with energy dispersive spectrometer (EDS). The cross-section samples were obtained by cutting hard carbons with high-energy argon ion beam. X-ray diffraction (XRD) analysis was performed on a Panalytical X'Pert PRO MPD instrument with Cu Kα radiation ($\lambda = 0.1541$ nm). The Raman spectrum was recorded on a Raman spectrometer (Renishaw 1000) with a He-Ne laser (50 mW, 514 nm) and a CCD detector. Nitrogen adsorption/desorption measurement was carried out with a Micrometrics Tristar 3000 analyzer at 77 K. Based on the adsorption data of isotherms, the pore size distributions were calculated by using Barrett-Joyner-Halenda (BJH) model, and the specific surface areas were calculated by the conventional Brunauer-Emmett-Teller (BET) method. The powder conductivities were determined on Mitsubishi Chemical MCP-PD51 at the pressure range from 12.73 to 63.66 MPa. The particle size distributions were measured by using a particle size instrument (Malvern company, Mastersizer 2000).

2.3 Electrochemical performance evaluation

For electrode preparation, the active material (91 wt%), carbon black (3 wt%), and polyvinylidene fluoride (PVDF, 6 wt%) were dispersed in N-methylpyrrolidone (NMP) by stirring. The obtained homogeneous slurry was coated on one side or double side of the collector and dried at 120 °C for 12 h. The collector is copper foil for hard carbon anode and aluminum foil for NCM523 (BTR company) cathode. The active material loading is 5.3 ± 0.3 mg cm⁻² for one-side-coated hard carbon electrodes used for half cells, and 10.6 ± 0.6 mg cm⁻² for double-side-coated hard carbon electrodes used for full cells, and 20~30 mg cm⁻² for double-side-coated NCM523 electrodes used for

full cells, respectively. The electrolyte is 1 M LiPF_6 (EC/PC/DMC= 1:1:1) solution and a microporous membrane (Celgard-2400) is the separator. For both half cells and full cells, the 2016-type coin cells and commonly used for the commercial vehicles 18650-type full cells were used, respectively, and assembled in an argon-filled glovebox with low moisture and oxygen (both less than 1 ppm) by pairing the hard carbon working electrode with a lithium sheet counter electrode or NCM523 cathode, respectively. The galvanostatic charge-discharge (GCD) curves and rate performance tests were conducted on an Arbin (BT2000) cell tester at 25 °C. In the GCD testing, the half cells were first charged to 5 mV at the rate of 0.1 C (nominal capacity= 400 mAh g^{-1}), and constant voltage charging at 5 mV was then carried out until the current was decreased to 0.3 mg cm^{-2} . Constant current (CC) discharging was performed at the rate of 0.1 C until 1.5 V was reached. The current voltammetry (CV) and electrochemical impedance spectroscopy (EIS) of half cells were detected on an electrochemical workstation (Solartron Instruments, 1470E). The EIS were collected at 50% state of charge (SOC) after two activation cycles at 0.1 C at the frequency of 0.1 Hz to 100 kHz with an amplitude of 10 mV.

3. RESULTS AND DISCUSSION

3.1 Materials characterizations

The structure and surface morphology of the biomass-derived hard carbon were first characterized by SEM. As shown in Figure 1, the surface of PSC is very smooth (Figure 1a and b). In contrast, the sample of PSC-C has a rough surface (Figure 1d and e). The cross-section SEM images (Figure 1c and f) were also taken from the fresh exposed surfaces after cutting hard carbons with high-energy argon ion beam. Obviously, PSC-C has a core-shell structure, indicating the successful coating (Figure 1f). The thickness of the coating layer is estimated to be 0.5~2 μm .

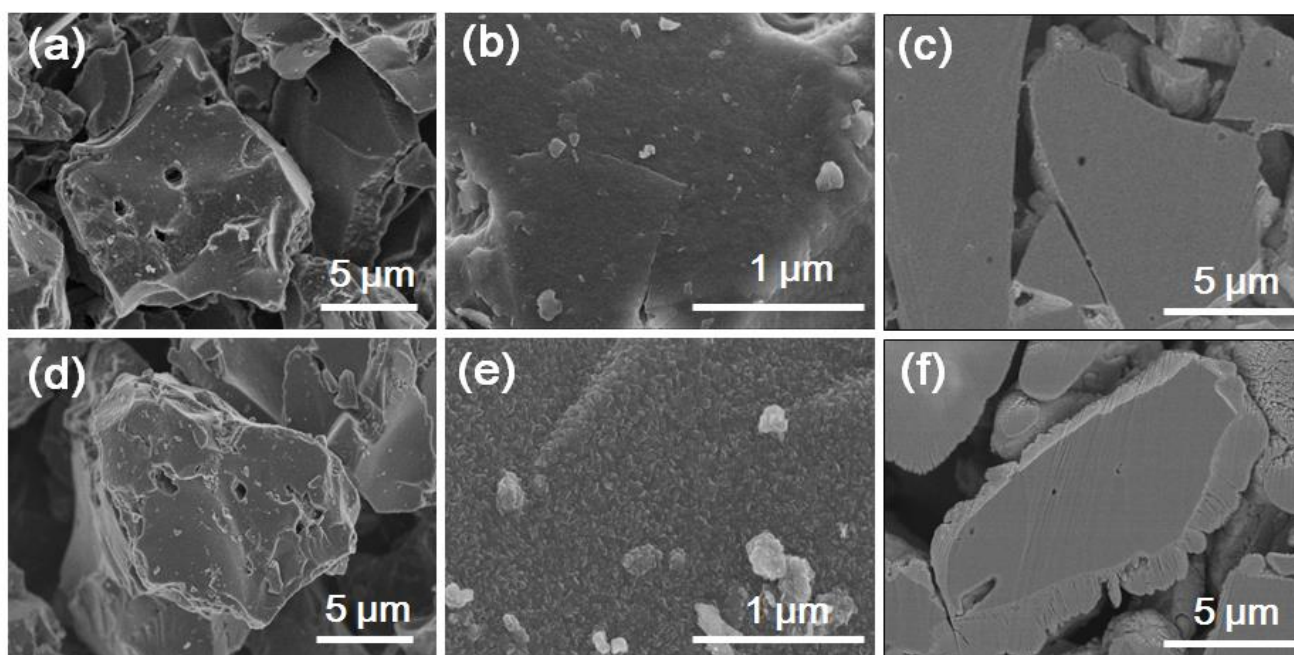


Figure 1. (a, b) SEM and (c) cross-section SEM images of PSC. (d, e) SEM and (f) cross-section SEM images of PSC-C.

The structure of PSC-C was further investigated by EDS measurement. Figure 2a shows that carbon element content in core region for the PSC-C is higher than that in the coating layer region. Conversely, oxygen element distributes mainly in coating layer region but less in core region (Figure 2b). The EDS spot-scanning demonstrates that the spectrum 1 located at the coating layer region of PSC-C exhibits a high oxygen content of 4.11 wt%, which is much more than that of the spectrum 2 and 3 (< 0.5 wt%) located at the core region (Figure 2f). However, carbon content of spectrum 1 (95.9 wt%) is less than that of spectrum 2 and 3 (> 99.5 wt%). This result is consistent to the EDS elemental mapping (Figure 2a-b). Therefore, PSC-C is covered with an oxygen-containing carbon coating layer which is believed to be derived from the oxygen-containing precursor of propionaldehyde.

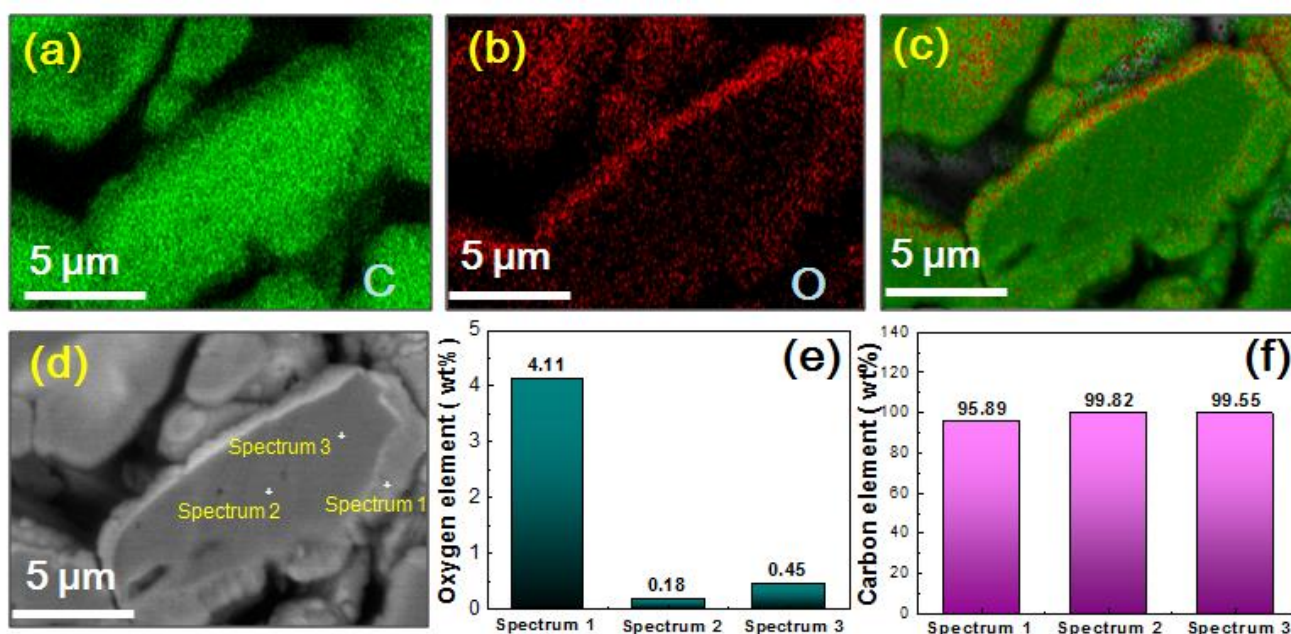


Figure 2. EDS elemental mapping images of PSC-C: (a) C mapping; (b) O mapping; (c) Overlap of C and O mapping; and (d-f) Elemental spot-scanning of C and O.

The particle size distributions of PSC and PSC-C were detected through particle size tester. As shown in Figure 3a, both PSC and PSC-C showed narrow distribution curves, indicating their uniform particle size. The median diameter of PSC-C ($D_{50} = 11 \mu\text{m}$) was slightly higher than that of PSC ($D_{50} = 9 \mu\text{m}$), suggesting that thickness of the carbon coating layer is $1 \mu\text{m}$ approximately. This is in good accordance with the SEM observation (Figure 2f). As presented in Figure 3b, powder conductivity curve of PSC-C is above that of PSC, implying that the CVD coating using propionaldehyde as a carbon precursor can considerably improve the conductive property of hard carbon and decrease the contact resistance between hard carbon particles. The porosities of PSC and PSC-C were assessed through the nitrogen adsorption/desorption measurements. Experimentally, the isotherms for PSC and PSC-C showed type IV curves with hysteresis loops [19, 20], indicating that their structures possess mesopores (Figure 3c). Furthermore, PSC-C gave the smaller hysteresis loop compared to PSC. This should be attributed to the formation of the dense carbon layer on the surface of the hard carbon

particles and resulting porosity reduction upon CVD. This can be further verified by the calculated BET specific surface area, which decreased from $2.40 \text{ m}^2 \text{ g}^{-1}$ for PSC to $1.67 \text{ m}^2 \text{ g}^{-1}$ for PSC-C. The XRD patterns (Figure 3e) of both PSC and PSC-C presented two broad diffraction peaks centered around 25° and 43° , which correspond to the (002) and (100) reflections of amorphous carbon materials [21], respectively. The interlayer spacing (D_{002}) of the hard carbon materials was calculated by Scherrer's formula. It is found that the D_{002} of PSC (0.383 nm) is almost identical to that of PSC-C (0.381 nm), suggesting the CVD coating would not alter the interlayer spacing. The Raman spectra of the samples are shown in Figure 3f. There are two obvious peaks at about 1350 cm^{-1} and 1580 cm^{-1} , which are corresponding to the D band and G band [22]. The I_D/I_G of PSC and PSC-C is 1.021 and 0.968, respectively, implying that the graphitization degree of hard carbon was improved slightly after coating.

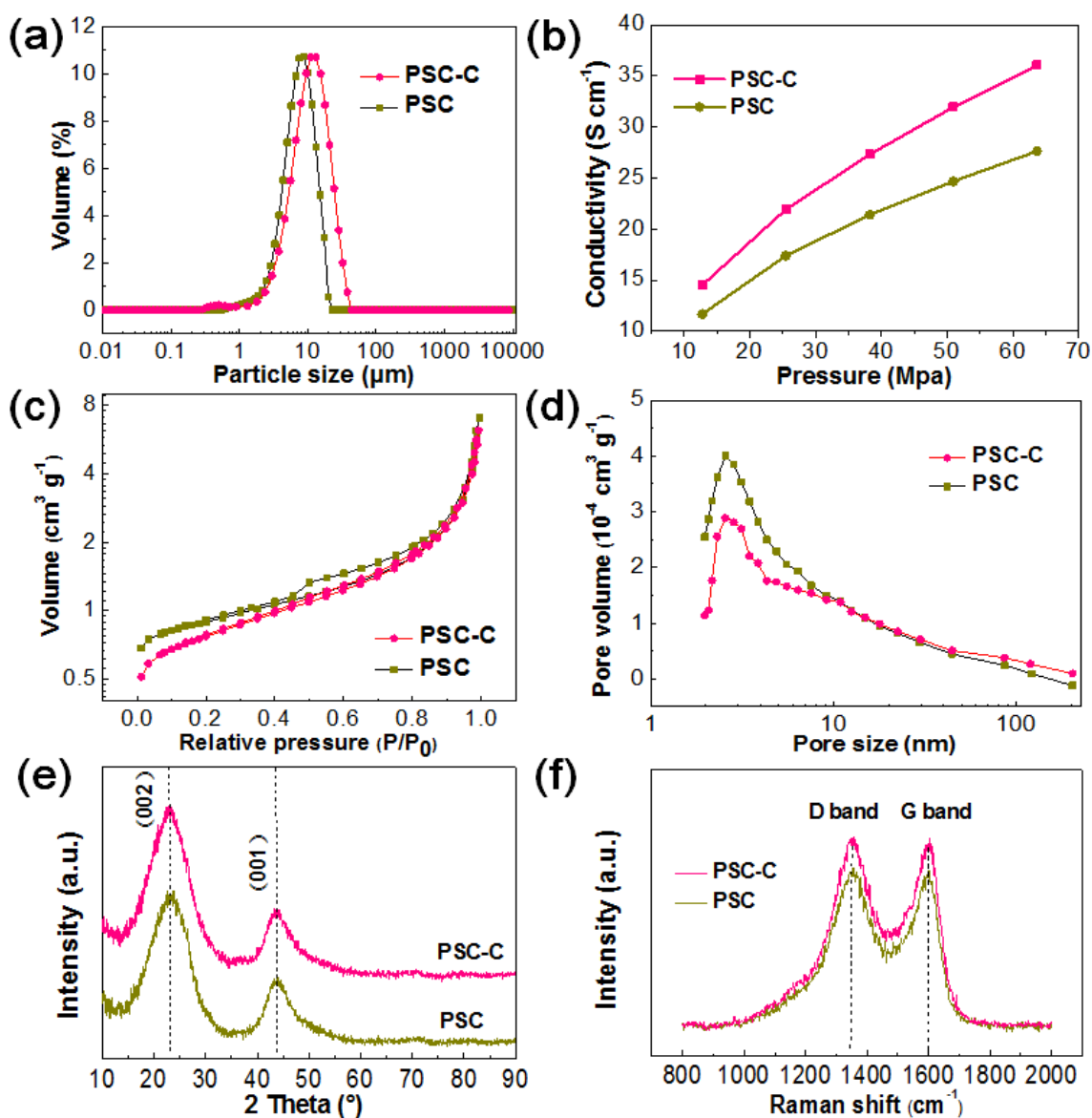


Figure 3. (a) Particle size distribution curves, (b) Powder conductivity curves, (c) Nitrogen adsorption-desorption isotherms, (d) BJH pore size distribution curves, (e) XRD patterns, and (f) Raman profiles of PSC and PSC-C.

3.2 Electrochemical characterizations

The loading mass of the active materials in the electrodes is an important factor. It is worth mentioning that the most publications report only specific capacity normalized by the mass of the active materials, and low areal mass loading helps to achieve the stable cycling and good rate performance. To obtain the electrochemical performance for the real practical applications, a high areal mass loading of over 5 mg cm^{-2} was used, which could achieve an areal capacity of about 2 mAh cm^{-2} for one-side-coated electrodes, close to the commercial areal capacity ($\sim 3 \text{ mAh cm}^{-2}$) for the one-side-coated graphite anodes. The lithium ion insertion-extraction behavior for hard carbons was first investigated by CV testing in the potential range of 0.01 V to 1.5 V. Figure 4a and b show the CV curves of the initial two cycles for PSC and PSC-C electrodes at a scan rate of 0.05 mV s^{-1} . The CV curves of PSC and PSC-C are alike in appearance. A broad peak at 0.4~1.1 V was detected in the first cathodic scan but disappeared in the subsequent cycle, which is attributed to the electrolyte decomposition and the formation of a solid-electrolyte interface (SEI) film on the hard carbon anodes [23]. However, PSC showed a broader and more obvious cathodic peak at 0.4~1.1 V (Figure 4a) than PSC-C, suggesting that PSC electrode consumed more lithium ions than PSC-C electrode during the SEI film formation [24].

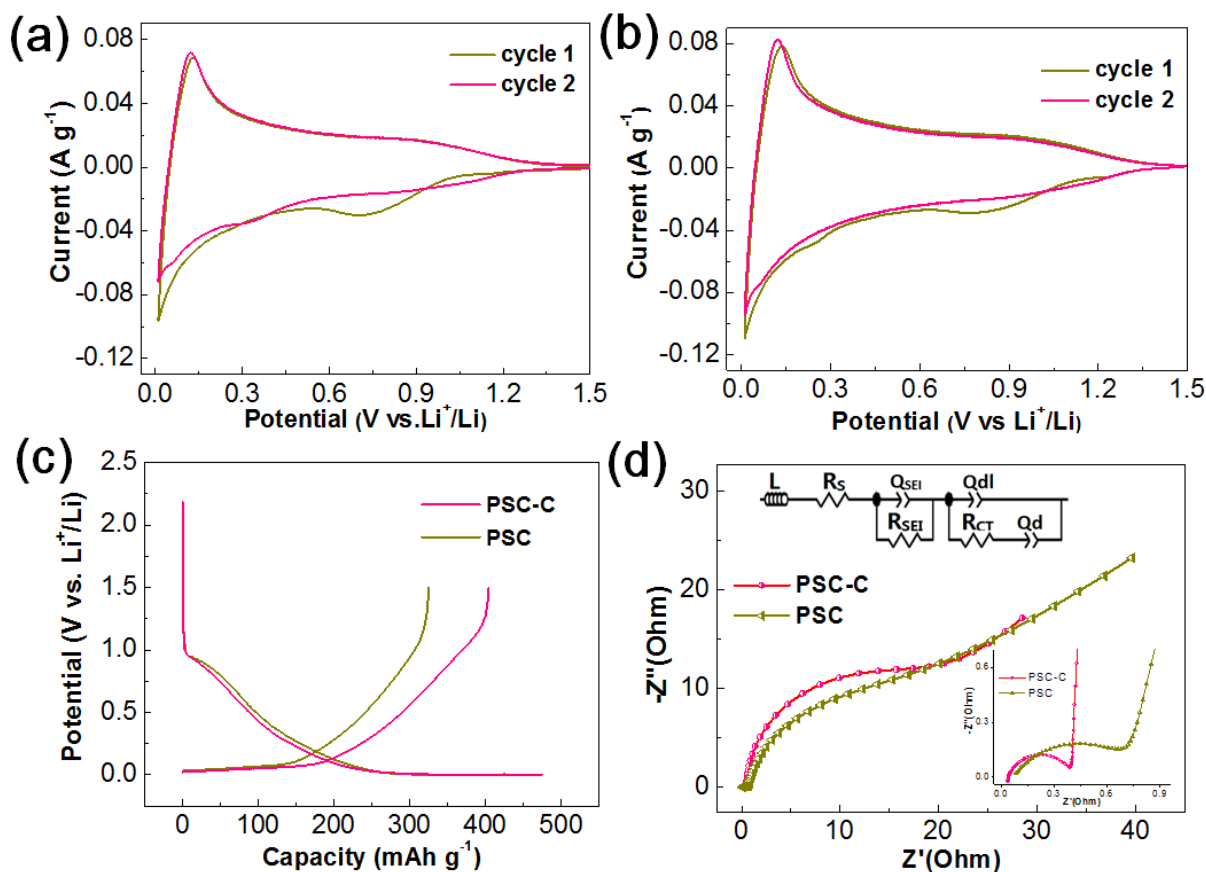


Figure 4. CV curves of (a) PSC and (b) PSC-C at a scan rate of 0.05 mV s^{-1} ; (c) First charge/discharge profiles of PSC and PSC-C at 0.1 C (nominal capacity= 400 mAh g^{-1}); (d) Nyquist plots of PSC and PSC-C at 50% SOC during the 3rd cycle and the equivalent circuit adopted for EIS fitting.

Figure 4c presents the galvanostatic charge-discharge (GCD) plots of PSC and PSC-C. The first irreversible capacity is 107.9 mAh g⁻¹ for PSC and 70.2 mAh g⁻¹ for PSC-C, respectively. This result indicated the carbon coating could remarkably decrease the irreversible capacity loss, consistent with the result of CV test. The decreased capacity loss is believed to be ascribed to the coverage of the inherently defect sites on the surface of hard carbon by CVD carbon coating, which isolated the direct contact of the defect-rich interface with the electrolyte. This is similar with the result reported previously [25]. Moreover, the superficial carbon coating layer can also construct a highly conductive network among individual hard carbon particles, which is believed to improve the homogeneity of the potential or current distribution in the electrodes and thus activate inert lithium storage sites. As a result, the first discharge (delithiation) capacity for PSC-C (404.3 mAh g⁻¹) was also higher than that of PSC (325.3 mAh g⁻¹). For a similar reason, the reversible capacity of hard carbon by thermal vapor decomposition (TVD) coating with benzene as precursor can also be increased [14]. However, benzene is carcinogenic material which is harmful to the users. Consequently, the ICE for hard carbon was significantly improved from 75.1% to 85.2% by CVD coating modification. As shown in Table 1, PSC-C exhibits excellent reversible capacity and the highest ICE when compared with other coated hard carbon served as anode materials for LIBs that were reported in literature.

Table 1. The comparison between PSC-C with other coated hard carbons for LIBs batteries.

Core material	Coating precursor	Coating method	Reversible capacity / mAh g ⁻¹	ICE	Ref.
NSF resin-derived carbon	benzene	TVD	536	76.6%	14
Hard carbon (Kureha Corp., Japan).	coal-tar pitch	mechanically mixing followed by heat-treatment	310	78.9%	16
Filter paper-derived carbon	CH ₄ (50%)-H ₂ (50%)	pressure-pulsed CVD	380	82.6%	17
Hard carbon (Akyung Petrochemical Co. Ltd. Korea)	microcrystalline graphite (10%) +pitch(20%)	mechanically mixing followed by heat-treatment	234	82.5%	26
Sugar-derived carbon	tetraethoxysilane (TEOS)	hydrothermal method	360	82.5%	27
Biomass-derived carbon	propionaldehyde	CVD	404	85.2%	this work

Nyquist plots for the PSC and PSC-C electrodes are similar in profile, as shown in Figure 4d. They all possessed a semicircle at the high frequency region and another semicircle at the medium frequency region, which related to the SEI resistance (R_{SEI}) and charge-transfer resistance (R_{CT}) [28, 29], respectively. The corresponding equivalent circuit is displayed in the inset of Figure 4d. As shown in Table 2, R_{SEI} of PSC-C electrode (0.37 Ω) is smaller than that of PSC one (0.70 Ω), which may be

related to the decreased SEI thickness for the former. Moreover, the PSC-C electrode also showed smaller R_{CT} than the PSC one (23.6 Ω vs. 31.5 Ω). The EIS analyses further verified that the formation of the dense and conductive carbon coating onto the defect-rich hard carbon materials suppressed the interfacial side reactions that led to the excessive growth of SEI film.

Table 2. EIS fitting results of PSC and PSC-C.

Sample	R_s (Ω)	R_{SEI} (Ω)	R_{CT} (Ω)
PSC-C	0.038	0.368	23.63
PSC	0.067	0.704	31.46

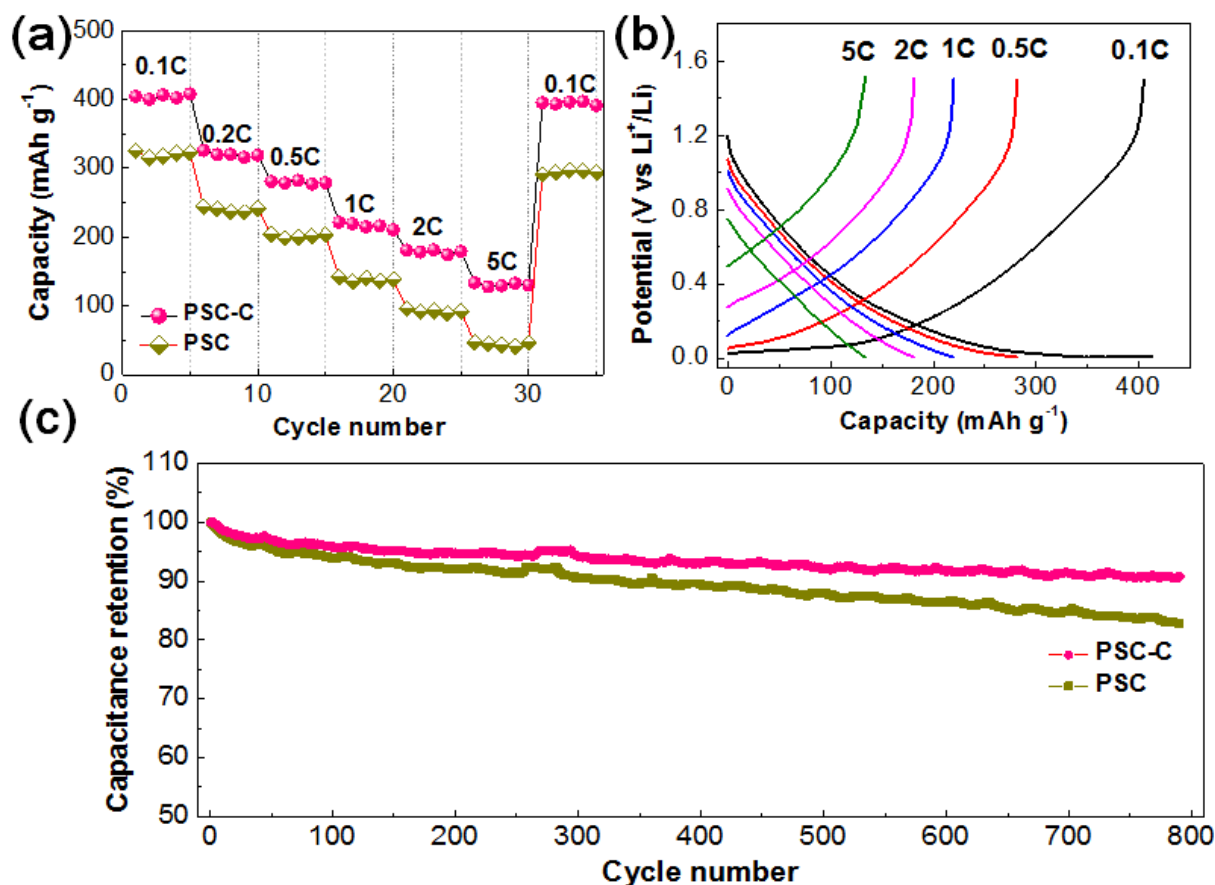


Figure 5. (a) Rate performance of PSC and PSC-C; (b) Charge/discharge profiles of PSC-C at different rate ranging from 0.1 C to 5 C; (c) Cycling performance of PSC and PSC-C at 6 C (assembled into 18650 type battery by massing with NCM523 cathode).

The rate performances are presented in Figure 5a. The PSC-C showed a slower capacity fading and delivered much higher reversible capacity (404.2 mAh g⁻¹ at 0.1 C, 219.4 mAh g⁻¹ at 1 C, 130.2 mAh g⁻¹ at 5 C) than those of PSC (325.2 mAh g⁻¹ at 0.1 C, 140.4 mAh g⁻¹ at 1 C, 43.5 mAh g⁻¹ at 5 C) at various rates. Moreover, after charge-discharge at the high rate of 5 C, the capacity of PSC-C nearly recovered 98% of its initial value at 0.1 C, while PSC only recovered 90%, suggesting the excellent reversibility of PSC-C. The improved rate capability of PSC-C may be attributed to the

reduction of polarization caused by its highly conductive carbon shell. The remarkable rate performance of PSC-C is further verified by little deviation from potential-capacity profiles at enhance current rates (Figure 5b).

To validate the practical feasibility of the material, 18650-type full cells with commercial NCM523 as a cathode and PSC-C (or PSC) as an anode were fabricated and tested at the rates of 6C/6C. As shown in Figure 5c, PSC-C exhibited a much higher capacity retention (91%) compared to that of PSC (83%) after 800 cycles, representative of an ultralow capacity decay of $\sim 0.012\%$ per cycle. Lee et al. [16] revealed that hard carbon with soft carbon coating layer showed improved Coulomb efficiencies compared with its control sample during cyclic test by half-cell. Yoshimi Ohzawa et al. [17] reported that hard carbon by pyrocarbon coating obtained a improved cycleability than that without coating. The enhanced cycling stability for PSC-C may be explained from two aspects: (1) the lower porosity of PSC-C with the coating layer reduced the formation of “dead lithium” during lithiation-delithiation; (2) the decreased defects on the surface of PSC-C restrained the repeated formation and decomposition of SEI film.

4. CONCLUSION

A novel hard carbon-based composite material with core-shell structure was prepared by the CVD carbon coating of a biomass-derived hard carbon with propionaldehyde as a precursor. The obtained hard carbon material covered with a uniform and thin carbon coating layer (0.5~2 μm) showed a large reversible capacity of 404.3 mAh g^{-1} and a high ICE of 85.2%. The full cell (18650 type) with the coated hard carbon material as anode exhibited outstanding cyclic stability, with a low capacity decay of $\sim 0.012\%$ per cycle over 800 charge-discharge cycles at high rates of 6C/6C. These results demonstrate that the CVD coating modification with propionaldehyde as a precursor is an efficient and promising method to synthesis hard carbon anode materials with superior electrochemical performances for large-scale applications.

ACKNOWLEDGEMENT

This study was financially supported by BTR new energy materials inc., Shenzhen, China.

References

1. C. D L, L. Charles and Z. Wen, *J. Power Sources*, 208 (2012) 74.
2. C. P. M Nagao, T Kamiyama and T Otomo, *J. Chem. Soc.*, 153 (2006) A914.
3. J. Li, R. Li and C. Bulin, *Int. J. Electrochem. Sci.*, 12 (2017) 4164.
4. M. Yoshio, H. Wang and K. Fukuda, *Angewandte Chemie*, 115 (2003) 4335.
5. Y. Xia, R. Fang, Z. Xiao, H. Huang, Y. Gan, R. Yan, X. Lu, C. Liang, J. Zhang, X. Tao and W. Zhang, *ACS Appl. Mater. Interfaces*, 9 (2017) 23782.
6. E. Buiel and J. R. Dahn, *Electrochim. Acta*, 45 (1999) 121.
7. L. Wang, Y. Liu, C. Chong, J. Wang and Z. Shi, J. Pan, *Mater. Lett.*, 170 (2016) 217.
8. Q. Zhang, H. Sun, X. Wang, Z. Zhu, W. Liang, A. Li, S. Wen and W. Deng, *Energy Technol.*, 1 (2013) 721.

9. P. Zhao, J. Tang and C. Wang, *J. Solid State Electrochem.*, 21 (2016) 555.
10. S. Sun, C. Y. Wang, M. M. Chen and M. W. Li, *Adv. Mater. Res.*, 724-725 (2013) 834.
11. N. Sun, H. Liu and B. Xu, *J. Mater. Chem. A*, 3 (2015) 20560.
12. T. Liu, R. Luo and S.-H. Yoon, I. Mochida, *Mater. Lett.*, 64 (2010) 74.
13. W. By Martin, B. Jürgen O. , S. Michael E. and N. k. Petr, *Adv. Mater.*, 10 (1998) 725.
14. M. Yoshio, H. Wang, K. Fukuda, T. Abe and O. Zempachi, *Chem. Lett.*, 32 (2003) 1130.
15. H.-Y. Leea, J.-K., Baeka, S.-W. Janga, S.-M. Leea, S.-T. Hongb, K.-Y. , Leeb and M.-H. Kimb, *J. Power Sources*, 101 (2001) 206.
16. J.-H. Lee, H.-Y. Lee, S.-M. Oh, S.-J. Lee, K.-Y. Lee and S.-M. Lee, *J. Power Sources*, 166 (2007) 250.
17. Y. Ohzawa, Y. Yamanaka, K. Naga and T. Nakajima, *J. Power Sources*, 146 (2005) 125.
18. E. B. and J. R. Dahnt, *J. Electrochem. Soc.*, 145 (1198) 1977.
19. D. Liu, C. Zeng, D. Qu, H. Tang, Y. Li, B.-L. Su and D. Qu, *J. Power Sources*, 321 (2016) 143.
20. D. Liu, G. Cheng, H. Zhao, C. Zeng, D. Qu, L. Xiao, H. Tang, Z. Deng, Y. Li and B.-L. Su, *Nano Energy*, 22 (2016) 255.
21. F. Su, C. K. Poh, J. S. Chen, G. Xu, D. Wang, Q. Li, J. Lin and X. W. Lou, *Energy Environ. Sci.*, 4 (2011) 717.
22. Y. An, Q. Zhu, L. Hu, S. Yu, Q. Zhao and B. Xu, *J. Mater. Chem. A*, 4 (2016) 15605.
23. D. Liu, X. Huang, D. Qu, D. Zheng, G. Wang, J. Harris, J. Si, T. Ding and J. Chen, *Nano Energy*, 52 (2018) 1.
24. J. Chen, Z. Mao, L. Zhang, D. Wang, R. Xu, L. Bie and B. D. Fahlman, *ACS nano*, 11 (2017) 12650.
25. F. Chevalliera, S. Gautiera, J.-P. Salvetat, C. Clinard, E. Frackowiak, J.-N. Rouzaud, F. Béguin, *J. Power Sources*, 97 (2001) 143.
26. J.-K. Kim, S.-T. Lee and G.-H. Kim, *Electrochim. Acta*, 11 (2014) 27.
27. Q. Wang, H. Li, L.-Q. Chen and X.-J. Huang, *Solid State Ionics*, 152 (2002) 43.
28. L. Zhang, K. Shen and W. He, *Int. J. Electrochem. Sci.*, 12 (2017) 10221.
29. L. Yao, Y. Wang and M.-W. Xiang, *Int. J. Electrochem. Sci.*, 12 (2017) 206.